Photoluminescent gold nanoclusters as two-photon excited ratiometric pH sensor and photoactivated peroxidase

Yuchi Cheng, Huangmei Zhou, Jinming Xu, Yu Zhao, Xihang Chen, Rodolphe Antoine, Meng Ding, Kun Zhang, Sanjun Zhang

Photoluminescent Gold Nanoclusters as Two-photon Excited Ratiometric pH Sensor and Photoactivated Peroxidase

Yuchi Cheng [a], *Huangmei Zhou* [a], *Jinming Xu* [a], *Yu Zhao* [a], *Xihang Chen* [a], *Rodolphe Antoine* [b*], *Meng Ding* [c], *Kun Zhang* [c,] *, *and Sanjun Zhang* [a, d,] *

[a] State Key Laboratory of Precision Spectroscopy, East China Normal University, No.500, Dongchuan Road, Shanghai 200241, China

[b] Institut Lumière Matière UMR 5306, Université Claude Bernard Lyon 1, CNRS, Univ Lyon, F69100 Villeurbanne, France

[c] Shanghai Key Laboratory of Green Chemistry and Chemical Processes, College of Chemistry and Molecular Engineering, East China Normal University, No.3663, North Zhongshan Road, Shanghai 200062, China

[d] Collaborative Innovation Center of Extreme Optics, Shanxi University, Taiyuan, Shanxi 030006, China

* Correspondence to R.A (email: rodolphe.antoine@univ-lyon1.fr), K. Z. (email: kzhang@chem.ecnu.edu.cn), and S.Z. (email: sjzhang@phy.ecnu.edu.cn)

Abstract

pH plays an important role in maintaining fundamental cellular functions, therefore it is of great significance to accurately measure pH value in living cells. Herein, we reported a two-photon excited ratiometric fluorescent pH sensor by combining L-cysteine-protected AuNCs (Cys@AuNCs) with fluorescein isothiocyanate (FITC). Cys@AuNCs were synthesized through a one-step self-reduction route and showed pH-responsive photoluminescence at 650 nm. Benefiting from the opposite pH response of Cys@AuNCs and FITC, the fluorescence ratio ($F_{515\ nm}/F_{650\ nm}$) of FITC&Cys@AuNCs provided a large dynamic range of 200-fold for pH measurement in the response interval of pH 5.0–8.0. Meanwhile, based on the excellent two-photon absorption coefficient of Cys@AuNCs, the sensor was expected to achieve sensitive quantitation of pH in living cells under two-photon excitation. In addition, colorimetric biosensing based on enzyme-like metal nanoclusters has attracted wide attention due to their low-cost, simplicity and practicality. It is crucial to develop high catalytic activity nanozyme from the viewpoint of practical application. The synthesized Cys@AuNCs exhibited excellent photoactivated peroxidase-like activity with high substrate affinity and catalytic reaction rate, promising for rapid colorimetric biosensing of field analysis and the control of catalytic reactions by photostimulation.

Keywords: gold nanoclusters, pH sensor, ratiometric fluorescence, two-photon excited imaging, photocatalysis

1. Introduction

In recent decades, metal nanoclusters (MNCs) composed of a metal core and a ligand shell have attracted extensive attention. With their core sizes comparable to the Fermi-wavelength of electrons, MNCs exhibit many unique molecule-like properties, such as discrete energy levels structure [1], photoluminescence [2], chirality [3] and magnetism [4], which resulted from the strong quantum confinement effect [5]. Owing to the advantages of size-sensitive photophysical properties, engineerable structural compositions, versatile surface groups and large surface-to-volume ratio, MNCs have made significant progress in the fields of optoelectronics, sensors, biomedicine and catalysis [6, 7].

Benefiting from the good biocompatibility, various MNCs-based luminescent probes have been developed for the detection of intracellular metabolites and physiological reactions [8]. The pH is an important indication for biochemical processes and pathological diagnostics because it plays a wide regulatory role in many cellular functions, such as ion transport, calcium regulation, cellular metabolisms and others [9]. In general, the cytosolic and extracellular pH under normal physiological conditions are 7.2 and 7.4, respectively [10]. Abnormal pH level may indicate diseases, including cancer [10] and Alzheimer's disease [11]. Therefore, accurate detection of the pH level in living cells is extremely crucial for understanding fundamental physiological processes. To date, many methods have been reported to detect the pH value including pH-sensitive microelectrodes, magnetic resonance, UV-vis absorption spectroscopy, fluorescence spectroscopy, etc. [12]. Fluorescent detection has the advantages of high spatial resolution and simple operation, which is a powerful tool for sensitive detection of pH in living cells. It was reported that MNCs have great potential for the fluorescent measurement of pH [13]. However, there are still some challenges in the applications of these fluorescent probes. First, it is difficult to quantitatively measure the pH value using a sensor with a single fluorescence emission peak. Second, the photoluminescence of most metal nanoclusters requires the excitation of UV-Visible light, thus leading to the interference of endogenous fluorescence and phototoxicity during cell imaging.

Much effort has been devoted to overcoming the challenges described above.

Ratiometric fluorescence measurements can eliminate the influence of measurement parameters and have been proved to be more suitable for quantitative detection in living cells. The ligands of nanoclusters provide abundant functional groups for conjugation with other fluorescent materials, allowing the design of ratiometric probes by introducing a reference signal, but the excited wavelengths were still UV-Visible light [14]. Fortunately, numerous publications have demonstrated that metal nanoclusters are promising candidates for two- and multi-photon excited fluorescence imaging, allowing the special design of two-photon excited fluorescent sensors [15-17]. Two-photon imaging is an effective strategy to extend the excitation wavelength from ultraviolet to near-infrared, enabling deeper tissue penetration and less endogenous fluorescence [18].

Besides of fluorescent biosensing, metal nanoclusters with enzyme-like properties have attracted wide attention as alternatives for natural enzymes in colorimetric sensing for point-of-care diagnosis. Peroxidase, especially horseradish peroxidase which can catalyze the oxidation of peroxide hydrogen, has been widely used in many fields, is a key component of enzyme linked immunosorbent assay (ELISA) [19]. However, the complex preparation and purification processes as well as strict storage conditions of natural enzymes largely limit their applications. Since Scrimin and co-workers discovered that thiol monolayer-protected gold nanoclusters can exhibited ribonuclease-like activity and proposed the concept of "nanozyme", many efforts have been devoted to studying catalytic properties of MNCs [20]. Nanoclusters with intrinsic peroxidase-like activity have received tremendous attention for rapid and convenient colorimetric detection owing to the advantages of low-cost, adjustable catalytic activity, high stability, and easy storage [21-22]. Moreover, most catalytic reactions start immediately after the addition of MNCs-based nanozymes, which is not convenient for the artificial regulation of the reaction process. Various nanozymes with photocatalytic properties based on metal nanoclusters have been reported, but their catalytic efficiencies need to be further improved because they usually required long time or high-power illumination [23, 24]. Therefore, it is of great significance to develop high-performance nanozymes with controllable catalytic properties, especially those that can be regulated via light irradiation.

In this article, a two-photon excited ratiometric fluorescent pH sensor was designed

through the combination of L-cysteine-protected AuNCs (Cys@AuNCs) and fluorescent dye FITC, namely FITC&Cys@AuNCs. As shown in scheme 1, two emission bands of the FITC&Cys@AuNCs showed opposite fluorescence responses to pH. Their fluorescence ratio improved the dynamic detection range by a factor of 200. FITC&Cys@AuNCs was capable of quantitatively measuring pH values in living cells under near-infrared light excitation. Moreover, Cys@AuNCs have excellent photoactivated peroxidase-like activity of high substrate affinity and catalytic reaction rate, making it possible to control catalytic reactions through light stimulation. This study not only provided a general design of two-photon fluorescence sensors using photoluminescent nanoclusters, but also demonstrated great potential of metal nanoclusters for photocatalysis. We hope that this study can contribute to further investigations and applications of metal nanoclusters in optical biosensors and biocatalysts.

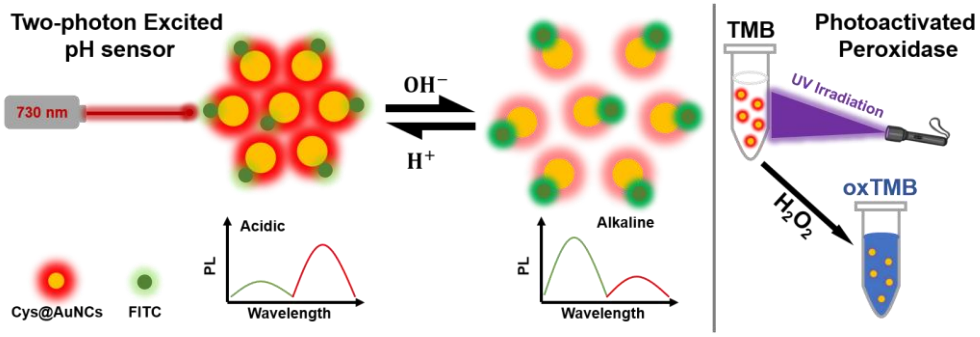

Scheme 1. Schematic representation of pH sensing of FITC&Cys@AuNCs and photoactivated peroxidase-like activity of Cys@AuNCs.

2. Experimental section

2.1. Materials and reagents

Gold (III) chloride trihydrate ($HAuCl_4 \cdot 3H_2O$, 99%), Dulbecco's Modified Eagle Medium (DMEM), superoxide dismutase and nigericin were purchased from Sigma-Aldrich Chemical Reagent Co., Ltd. (Shanghai, China). Rhodamine 6G, Fluorescein isothiocyanate (FITC), 3,3-,5,5-tetramethylbenzidine (TMB), EDTA, t-butanol, Triton X-100, DMSO and H_2O_2 (30 wt%, aqueous) were obtained from Aladdin Bio-Chem Technology Co., Ltd. (Shanghai, China). Metal salts, amino acids, NaCl, NaOAc, KCl, Na_2HPO_4 and K_2HPO_4 were bought from Sinopharm Chemical Reagent Co., Ltd. (Shanghai, China). Glucose and methyl thiazolyl tetrazolium (MTT) were obtained from Tokyo Chemical Industry Co., Ltd.

HEPES free acid was purchased from Amresco (Shanghai, China). Dialysis tube (MWCO: 1000 Da) was obtained from VAKE Corporation. All chemicals from commercial sources were used without further purification. All aqueous solutions were prepared by Ultrapure Millipore water system (18.2 MΩ·cm).

2.2. Instrumentation

The absorption spectra were performed with a double beam TU-1901 UV–Vis spectrometer (PERSEE, China). All steady-state luminescence spectra measurements were carried out on a FluoroMax-Plus fluorescence spectrometer (Horiba, Japan). Luminescence lifetimes were measured with a homebuilt time-correlated single photon counting system. The two-photon absorption coefficients were measured by the self-built Z-Scan system. Transmission electron microscopic (TEM) images were collected on JEM-2100F transmission electron microscope (JEOL, Japan). Size distribution in solution were obtained from Nano ZS3600 laser dynamic scatterometer (Malvern, UK). Fourier transform infrared (FTIR) spectra were performed with a NICOLET iS10 Infrared Spectrometer (Thermo Fisher Scientific, USA). XPS spectra were collected on AXIS SUPRA X-ray photoelectron spectroscope (Kratos, UK). All experiments were carried out at room temperature unless otherwise noted.

2.3. Synthesis of Cys@AuNCs and FITC&Cys@AuNCs

The Cys@AuNCs were synthesized according to a reported method with a little modulation [46]. In a typical experiment, aqueous $HAuCl_4$ solution (5 mL, 10 mM) was mixed with Cys solution (5 mL, 50 mM) under vigorous stirring for 2 min. Then 200 μL NaOH solution (1 M) was added, and the mixture was stirred at 60 °C for 3 h. Finally, the color of the solution changed from light yellow to milky. The synthesized Cys@AuNCs were dialyzed against ultrapure water for 24 h using dialysis tube (MWCO: 1000 Da).

To prepare FITC&Cys@AuNCs, FITC in ethanol (1000 μM) was added to Cys@AuNCs aqueous solution and stirred at room temperature in the dark for 12 h. FITC bound to Cys@AuNCs through the reaction between the isothiocyanate group and the amino groups of AuNCs. The prepared final solution was dialyzed for another 24 h and stored at 4 °C.

2.4. Two-photon excited pH ratiometric imaging in living cells

HeLa cells were incubated with 1 mL of fresh DMEM medium containing FITC&Cys@AuNCs for 1 h at 37 °C. Prior to imaging, cells were washed for three times with 10 mM PBS (137 mM NaCl, 2.7 mM KCl, 10 mM Na_2HPO_4, 2 mM K_2HPO_4, pH 7.4) and treated with 1 mL high-K^+ buffer (120 mM KCl, 1 mM $CaCl_2$, 30 mM NaCl, 0.5 mM $MgSO_4$, 1 mM NaH_2PO_4, 5 mM glucose, 20 mM HEPES, and 20 mM NaOAc) solutions of various pH values (6.0, 6.5, 7.0, 7.2, 7.5 and 8.0) containing 10 μM nigericin. FITC&Cys@AuNCs-loaded cells were imaged on a two-photon excitation confocal scanning microscope (TCS SP8, Leica microsystems, Germany) equipped with a pulsed laser (Chameleon Ultra II, COHERENT, USA) upon excitation at 730 nm. The fluorescence emission was detected at the range of 490–550 nm and 600–660 nm. The fluorescence images were processed using ImageJ and MATLAB software.

2.5. Catalytic oxidation of TMB

The TMB oxidation reaction was performed to investigate the peroxidase-like catalytic activity of Cys@AuNCs. In a typical experiment, 10 μL of TMB (50 mM) and 10 μL of H_2O_2 (30 wt%, aqueous) were added to 480 μL of PBS buffer, followed by 20 μL of nanocluster solution. The color change of the mixture was quickly observed by irradiation with a 365 nm UV lamp, and the UV-Vis absorbance was further measured to monitor the oxidation reaction.

3. Results and Discussion

3.1. Characterization of Cys@AuNCs and FITC&Cys@AuNCs

The photophysical properties of MNCs are correlated with morphology and size, and the TEM image showed that the synthesized Cys@AuNCs exhibited obvious cluster structure and good uniformity with an average diameter of ~3.6 nm (Fig. 1a). As shown in Fig. 1b, the maximum absorption of Cys@AuNCs appeared at 370 nm, and there was no characteristic surface plasmon resonance (SPR) peak (~520 nm) belonging to gold nanoparticles. These results indicated the formation of gold nanoclusters. When excited at 365 nm, Cys@AuNCs exhibited obvious photoluminescence at around 650 nm (Fig. 1c), and the fluorescence quantum yield of Cys@AuNCs was 2.3% at pH 6.0 (calibrated with rhodamine 6G as reference, Fig. S1). To construct ratiometric pH sensor, FITC was introduced into the NCs

system as another sensing unit. FITC showed different optical properties from Cys@AuNCs, with an absorption peak at ~490 nm and green fluorescence at ~520 nm (Fig. 1b and 1c). After combining with FITC, the absorption peak of Cys@AuNCs at ~370 nm maintained and new absorption peak originated from FITC at ~490 nm occurred (Fig. 1b). Upon excitation at 365 nm, the final product (denoted as FITC&Cys@AuNCs) exhibited fluorescence emission at ~520 nm and ~650 nm, indicating the existences of FITC and Cys@AuNCs (Fig. 1c). FTIR spectra were measured to further analyze the composition (Fig. 1d). The band at around 2540 cm^{-1} in the FTIR spectrum of Cys was assigned to the stretching vibration of S-H [14], which disappeared in the spectrum of Cys@AuNCs due to the formation of Au-S bonds. The free N=C=S group of FITC showed a characteristic peak at 2040 cm^{-1} [14], while there was no similar peak in the FTIR spectrum of FITC&Cys@AuNCs, confirming the covalent combining between FITC and Cys@AuNCs.

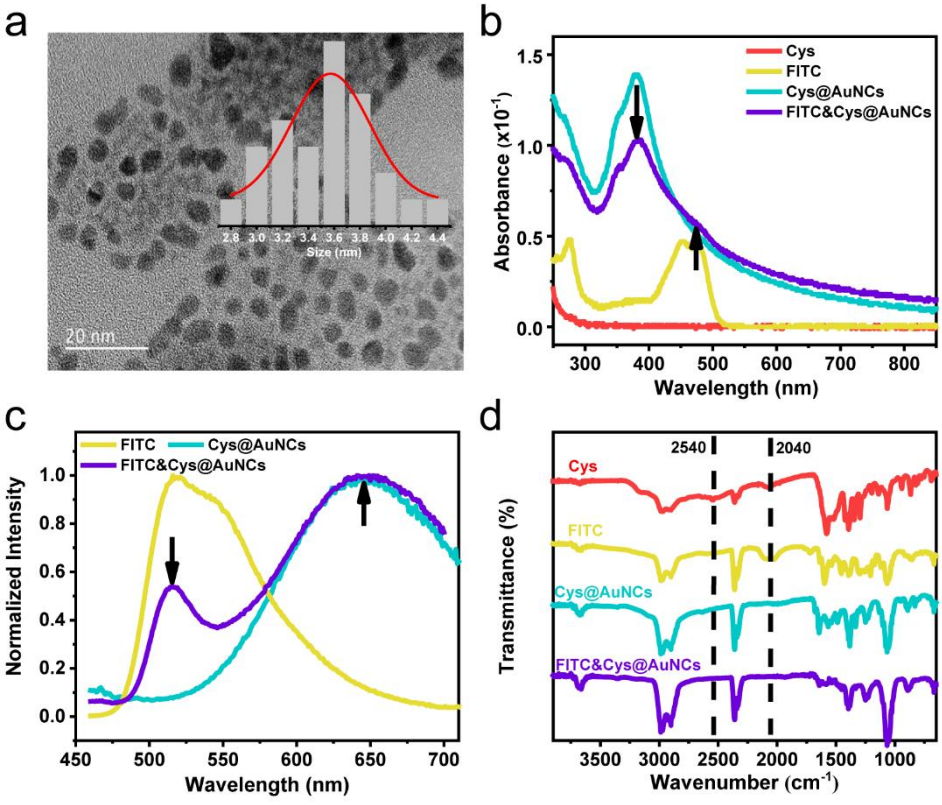

Fig. 1. (a) TEM image of Cys@AuNCs. (b) UV-vis absorption spectra of Cys, FITC, Cys@AuNCs and FITC&Cys@AuNCs. (c) Normalized photoluminescence (PL) spectra of FITC, Cys@AuNCs and FITC&Cys@AuNCs (excited at 365 nm). (d) FTIR spectra of Cys, FITC, Cys@AuNCs and FITC&Cys@AuNCs, the spectra were vertically offset for clarity.

3.2. Sensing performance of Cys@AuNCs and FITC&Cys@AuNCs for pH detection under one-photon excitation

The photoluminescence of Cys@AuNCs in different pH buffers were examined. As shown in Fig. S2, the fluorescence spectra varied with pH, and the fluorescence intensity decreased when the pH value increased from 6.0 to 11.0. TEM images were adopted to investigate the aggregation states of Cys@AuNCs at different pH values. It was observed that Cys@AuNCs were more dispersed in alkaline buffer than in acidic condition (Fig. S3). Meanwhile, the Cys@AuNCs solution appeared obvious suspended matter at pH 6.0, while the solution was relatively clear at pH 11.0. Dynamic light scattering was used to measure the size distribution of Cys@AuNCs in different pH buffers. The larger size of Cys@AuNCs in acidic solution further confirmed the formation of nanoparticles with low solubility, which were produced by the aggregation of the nanoclusters (Fig. S4). The time-resolved fluorescence spectra of metal nanoclusters were also measured (Fig. S5). According to the fitting results in Table S1, the average fluorescence lifetime of Cys@AuNCs changed from 0.9 μs to 0.8 μs with the increase of pH. Meanwhile, the proportion of fast-decay component (~ 1.0 ns) increased, and the proportion of other slow-decay components (> 1.0 ns) decreased. These results demonstrated that strong photoluminescence under acidic condition was owing to the aggregation of Cys@AuNCs. The nanoclusters were dissolved as isolated species under alkaline conditions, involving flexible molecular conformation and arrangements, and the non-radiative decay pathway originating from intramolecular motions was dominant. On the contrary, the intramolecular vibration and rotation of the ligands were restricted in acidic solutions, resulting in the reduction of the non-radiative relaxation as well as enhanced fluorescence, which was consistent with the reported pH-induced aggregation behaviors of MNCs [25].

Though the photoluminescence intensity of Cys@AuNCs was sensitive to pH, such a single emission intensity change may be largely effected by locally uneven probe concentration during cell imaging and interfere with pH measurements. Instead, ratiometric fluorescence probe have proved to provide a self-calibration of two emission peaks to eliminate the aforementioned interference and realize quantitative measurement of pH. Inspired by the advantage of ratiometric probe, we introduced FITC as the reference signal.

The standard pH titration of FITC&Cys@AuNCs was performed in PBS buffer from pH 5.0 to 8.0. As shown in Fig. 2a, the luminescence intensity of FITC and Cys@AuNCs was both responsive to pH. As the pH increased, the fluorescence intensity of FITC at 515 nm was enhanced while the red photoluminescence belonging to Cys@AuNCs diminished. The sensor also exhibited color-switchable fluorescence emission at different pH values under UV lamp, meaning that it can also be used as a visual pH indicator in solution (Fig. S6). The pH response interval of FITC&Cys@AuNCs was 5.0 – 8.0, which was consistent with the physiological range, implying that this sensor had great potential for pH detection *in vivo*. Benifiting from the opposite changing trends towards pH of two emission peaks, their fluorescence ratio ($F_{515\ nm}/F_{650\ nm}$) provided a large dynamic (~200-fold, from 0.2 to 40) for pH measurements (Fig. 2b). As far as we know, the ratio variation of the previously reported ratiometric pH sensors were only a few or a dozen times within the measurement range, FITC&Cys@AuNCs can provide a much more sensitive for quantitative measurement of pH (Table S2).

The complexity of the intracellular environment is a great challenge for application of biosensors in biological systems. It was known that the presence of various ions, amino acids and proteins in cellular matrix may affect the photoluminescence of the sensor. Relevant selectivity experiments were carried out to further verify the practicality of FITC&Cys@AuNCs. As shown in Fig. 2c, 11 common metal ions had negligible effect on the fluorescence ratio of FITC&Cys@AuNCs. Similarly, the fluorescence ratio of probe also nearly unchanged when the probe coexisted with several typical amino acids and proteins (Fig. 2d). These results validated that reliable pH values could be obtained by the developed ratiometric sensor in complicated biological system. The photostability and fluorescence reversibility response are necessary conditions for continuous and dynamic monitoring of pH using fluorescence probes. After being exposed to 365 nm UV light for 1 hour, the fluorescence ratio of FITC&Cys@AuNCs changed less than 5% (Fig. 2e), suggesting that the probe was suitable for long-term sensing of pH under physiological conditions. FITC&Cys@AuNCs also exhibited a highly reversible response when the pH switched for three cycles (Fig. 2f), enabling real-time monitoring of pH fluctuations.

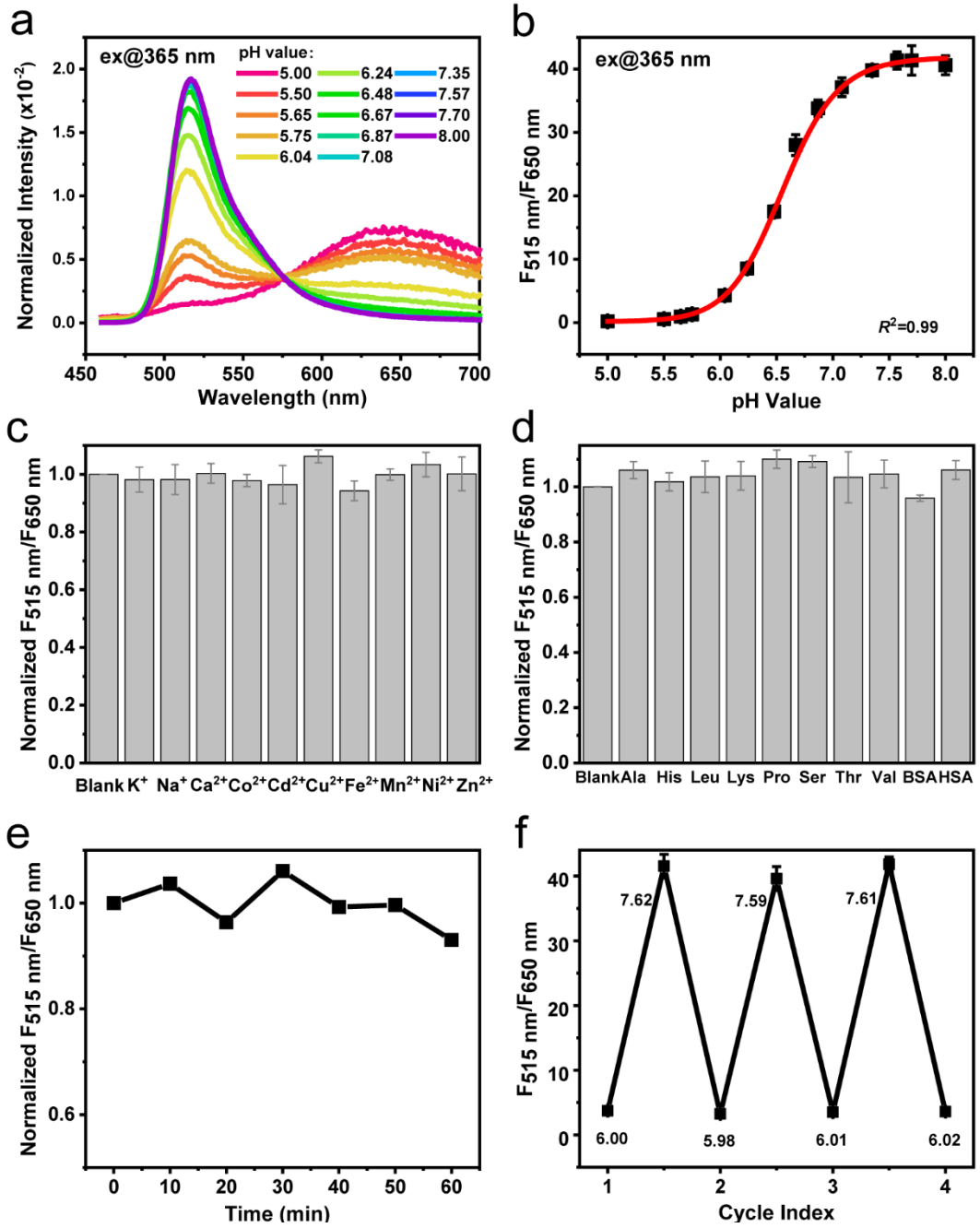

Fig. 2. (a) The intensity normalized photoluminescence spectra of the FITC&Cys@AuNCs in buffer of pH from 5.0 to 8.0 (excited at 365 nm). (b) Plot of $F_{515\ nm}/F_{650\ nm}$ as a function of pH (excited at 365 nm). (c) Effect of metal ions and (d) amino acids and proteins on probe response (1 mM for K^+, Na^+, Ca^{2+}, 10 μM for Co^{2+}, Cd^{2+}, Cu^{2+}, Fe^{2+}, Mn^{2+}, Ni^{2+}, Zn^{2+}, amino acids and proteins; excited at 365 nm, normalized by the ratio of blank sample). (e) The photostability of FITC&Cys@AuNCs when exposed to 365 nm for 1 h, normalized by the ratio at the initial time). (f) The fluorescence reversibility response of FITC&Cys@AuNCs to pH (excited at 365 nm). Error bars: standard deviation, n = 3.

3.3. Validating the practicability of FITC&Cys@AuNCs under two-photon excitation

Biocompatibility is an important parameter to evaluate the performance of fluorescence sensor. To evaluate the cytotoxicity of FITC&Cys@AuNCs, the standard MTT proliferation experiments were operated in HeLa cells. As shown in Fig. S7, the HeLa cells maintained nearly 85% viability after incubation with different concentrations of FITC&Cys@AuNCs for 24 h, suggesting that FITC&Cys@AuNCs can be used as a bioimaging sensor.

As we all know, fluorescence imaging in near-infrared window is more suitable for living cells. Designing fluorescent probes with near-infrared excitation or emission wavelengths is a research hotspot. Two-photon excitation fluorescence is a convenient strategy to extend the excitation wavelength to the near-infrared window. Considering the excellent nonlinear optical properties of metal nanoclusters [15], we designed the FITC&Cys@AuNCs as two-photon excited ratiometric sensor to avoid endogenous fluorescence and phototoxicity caused by UV-VIS excitation light. The two-photon absorption coefficient of Cys@AuNCs was 2.45×10^{-11} cm/W when the concentration of Au atoms was 0.5 mM. As well known that each metal nanocluster contained multiple gold atoms, meaning that in this case the concentration of the cluster was much lower than 0.5 mM. But the two-photon absorption coefficient of Cys@AuNCs was 3 times larger than that of 1 mM R6G (2.45×10^{-11} cm/W *v.s.* 8.4×10^{-12} cm/W), indicating that Cys@AuNCs has greater two-photon absorption cross section (Fig. S8). To explored the performance of FITC&Cys@AuNCs under two-photon excitation, we first measured the two-photon excitation spectra of FITC and Cys@AuNCs. They exhibited two-photon excited fluorescence in both green and red detection channels, and the optimal excitation wavelength was 730 nm in the range of 700-900 nm (Fig. S9). Subsequently, FITC&Cys@AuNCs were tested for pH titration experiments under two-photon excitation. It could be found that the fluorescence spectra varied with pH values, and meanwhile the pH response range and fluorescence ratio changes were basically consistent with those results under one-photon excitation (Fig. 3a and 3b), indicating that FITC&Cys@AuNCs could be used for two-photon fluorescence imaging of pH. The spectral curves were slightly different between one- and two-photon excitation because of the different detector performance of two-photon confocal imaging system and fluorescence spectrometer. Compared with other nanomaterial-based

two-photon excited pH sensors (Table 1), the FITC&Cys@AuNCs has distinct advantages, including ratiometric fluorescence detection, larger dynamic change range, and wider physiological pH response, which can be suitable for sensitive quantitation of pH in living cells.

Table 1. An overview of recently reported nanomaterial-based two-photon excited fluorescent pH sensors.

Materials	Method	pH Response interval	Dynamic range	Refs
FITC-PFO conjugated polymer NPs	Emission Ratiometric	4.0-9.0	~6-fold	[26]
Carbazole−oxazolidine π-conjugated system	Emission Ratiometric	4.5-9.2	~14-fold	[27]
Carbon dot-based Inorganic–Organic Nanosystem	Intensiometric fluorescence	6.5-8.5	~2.6-fold	[28]
Nano-PEBBLE sensor	Excitation Ratiometric	6.0-8.0	~5-fold	[29]
Dye-concentrated organically modified silica nanoparticles	Emission Ratiometric	4.0-8.0	~3.4-fold	[30]
FITC&Cys@AuNCs	Emission fluorescence	5.0-8.0	~72-fold	This Work

Two-photon excitation microscopy was employed for the visual analysis of pH values of HeLa cells. Before fluorescence imaging of pH in living cells, the fluorescence intensity of cells with different incubating times and probe concentrations was measured by fluorescence microscopy to investigate the cell internalization of the probe. Previous report suggested that the cellular internalization of photoluminescent gold nanoclusters is through an endocytotic uptake mechanism [31]. To obtain bright fluorescence signals, HeLa cells were firstly treated with a relatively high concentration of sensors (100 μg/mL) with different times, and the reasonable incubation time was 1h (Figure S10a). The cells were furtherly incubated with different concentrations of FITC&Cys@AuNCs for 1h to receive that high-quality images while minimizing cytotoxicity (Figure S10b). Subsequently, Two-photon excited confocal imaging of cells was performed under optimal conditions. As shown in Fig. 3c, FITC&Cys@AuNCs still exhibited stable fluorescence in the cellular environment. The pH calibration curve in living cells was obtained by treating FITC&Cys@AuNCs-loaded HeLa

cells with high-K^+ solutions containing nigericin (Fig. 3d and Fig. S11). The fluorescence intensities of 490-550 nm (F_{Green}) and 600-660 nm (F_{Red}) were recorded to calculate the fluorescence ratio with the excitation at 730 nm. Nigericin was used to equilibrate the intracellular and extracellular pH. As shown in Fig. 3c, the average emission ratio F_{Green}/F_{Red} of HeLa cells incubated in standard DMEM culture medium was 2.3±0.1. Then the actual pH value calculated from the calibration curve was about 7.4±0.1, which was consistent with the typical value of the cells in the standard culture environment [32]. In general, the results of the two-photon cell imaging experiments demonstrated that FITC&Cys@AuNCs were potential two-photon excited ratiometric pH sensors.

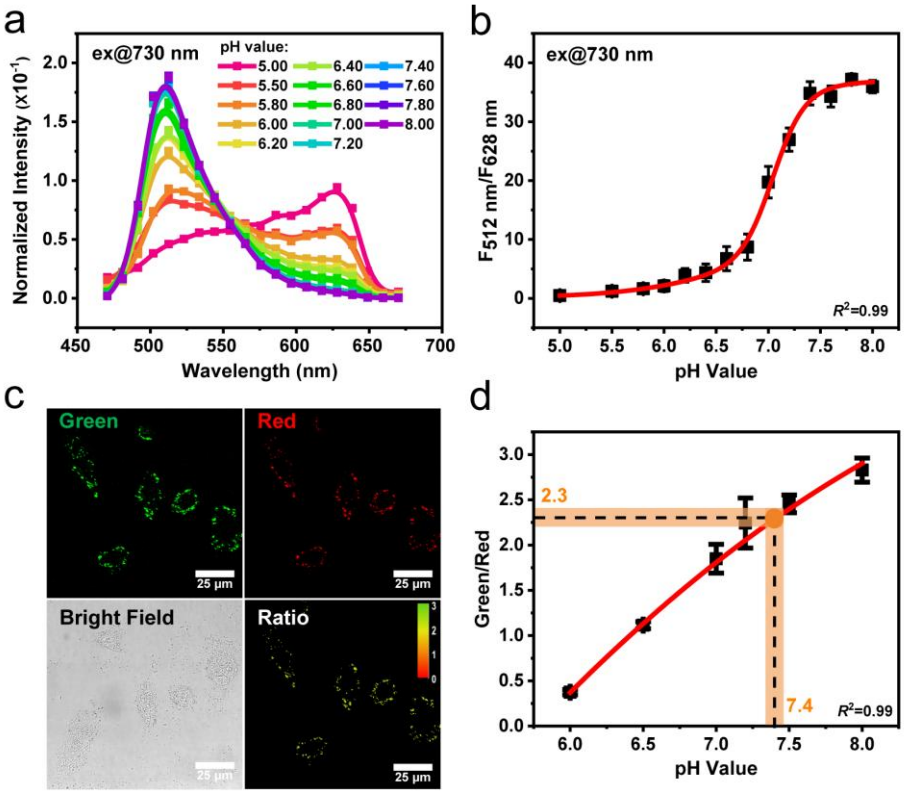

Fig. 3. (a) Two-photon fluorescence spectra of the FITC&Cys@AuNCs at different pH values (excited at 730 nm); (b) Plot of F_{512}/F_{628} as a function of the pH (excited at 730 nm). (c) Confocal fluorescence images of HeLa cells incubated with DMEM medium containing FITC&Cys@AuNCs (green channel: 490 nm-550 nm, red channel: 600 nm-660 nm, excited at 730 nm, scale bar: 25 μm); (d) The pH calibration curve of FITC&Cys@AuNCs in HeLa cells (excited at 730 nm). Error bars: standard deviation, n = 3.

3.4. The photoactivated peroxidase-like activity of Cys@AuNCs

The tetramethylbenzidine (TMB) oxidation reaction was selected as the model to study the photoactivated catalytic ability of Cys@AuNCs. TMB and H_2O_2 are usually used as substrates for colorimetric biosensing. In the presence of catalyst, the solution turns blue due to the TMB-derived oxidation products and the characteristic absorption peak is monitored at 650 nm. As shown in Fig. 4a, when Cys@AuNCs, H_2O_2 and TMB were mixed at room temperature, there was basically no change in the absorption spectrum even after 10 minutes. When exposed to the 365 nm UV lamp, the solution changed to blue within 1 min, and the absorption spectrum showed a peak at 650 nm originating from the oxidized TMB (oxTMB). And it was worth noting that the solution of TMB and H_2O_2 remained colorless when lacking of either Cys@AuNCs or 365 nm UV irradiation (Fig. 4a and Fig. S12). Therefore, it could be confirmed that Cys@AuNCs played the same role as horseradish peroxidase in TMB oxidation. What's more, compared to the natural horseradish peroxidase, the photoactivated enzyme-like activity of Cys@AuNCs make the catalytic reactions easily regulated by the on/off state of light stimulation.

Subsequently, we measured the catalytic rate of Cys@AuNCs to TMB. The catalytic reaction could be completed rapidly within 90 seconds under the UV lamp (Fig. 4b), at lower light irradiation intensity and shorter time than previously reported gold nanocluster-based photocatalysis (90s *V.S.* 30min, and 18 mW/cm^2 *V.S.* 30 mW) [23]. The Michaelis–Menten constant (K_m) and maximum reaction rate V_{max} are used to evaluate enzymatic catalytic properties, and can be obtained by Lineweaver–Burk plot [33]:

$$\nu = V_{max} \times \frac{[S]}{K_m + [S]}$$

where ν is the initial rate and $[S]$ is the concentration of the substrate. The apparent steady-state kinetic parameters were determined using steady-state kinetics assay (Fig. 4c). The K_m and V_{max} of Cys@AuNCs with TMB as substrate were 92.63 μM and 4.63 μM·s^{-1}, suggesting the relatively high peroxidase-like activity of the synthesized Cys@AuNCs compared to the previous analogues (Table S3**)**.

Furthermore, the influence of irradiation with different wavelengths on the catalytic activity of Cys@AuNCs were investigated. The results showed that only 365 and 400 nm could induce the appearance of characteristic absorption peaks at 650 nm, indicating the

activation of peroxidase-like activity of the nanoclusters, while the redder lights irradiation made no effect on the reaction (Fig. 4d). The absorption spectrum reflects the ability of light of different wavelengths to pump the ground state molecule into an excited state. The activation efficiency of these wavelengths on the peroxidase-like activity of Cys@AuNCs was consistent with the absorption spectrum of Cys@AuNCs (Fig. 4e), revealing that the catalytic activity of the nanoclusters required the participation of excited states with electron-hole separation.

The effect of pH on the peroxidase-like activity of Cys@AuNCs were also explored. As depicted in Fig. 4f, the solution exhibited obviously blue under acidic conditions and was still colorless at pH 9.0 for the same light irradiation time. And the absorbance at 650 nm decreased significantly as the pH value increased, indicating the reduction of oxTMB produced. The above results indicated that the peroxidase-like activity was highly dependent on pH, which was interestingly consistent with the fluorescence response of Cys@AuNCs to pH (Fig. S2). It has been reported that the catalytic activity of gold nanoclusters was affected by the valence of Au on their surface [34]. XPS was performed to characterize the valence states of Au in Cys@AuNCs at different pH values. As shown in Figure S13, the binding energy of both Au 4f5/2 and Au 4f7/2 in Cys@AuNCs were located at 88.1 and 84.4 eV at different pH values. The similar binding energy indicated that the pH-dependent differences in photocatalytic activity of Cys@AuNCs were not due to the valence change of Au in the nanoclusters. Based on the photocatalytic results under different irradiation wavelengths and pH conditions, we proposed the possible mechanism of photoactivated catalysis. As previously reported, H_2O_2 might be absorbed onto the surface of AuNCs-based nanozymes during the catalytic reaction [24, 25]. And the nanoclusters were excited to singlet excited state through UV light irradiation, generating separated electron-holes between the LUMO and HOMO energy levels. The long-lived triplet excited state could be formed by the singlet excited state through intersystem crossing, which provided the longer electron–hole separation lifetime so that photogenerated electrons and holes could be efficiently transferred to the surface and interact with the surrounding H_2O_2 [24, 25]. Then the O-O bonds of H_2O_2 were broken, leading to the production of reactive oxygen species. The generated reactive oxygen species could be further stabilized via the exchange of the electron with the AuNCs,

and oxidized TMB to oxTMB, causing the solution to change from colorless to blue [24, 25]. As described before, the diminished fluorescence in the alkaline environment was due to the return of nanoclusters from excited state to ground state mainly through nonradiative transitions. In this case, the short electron-hole separation lifetime may inhibit peroxide-like activity of the AuNCs. Furthermore, the superoxide dismutase (SOD), EDTA and t-butanol were employed as scavengers of the relevant reactive species including superoxide anions ($O_2^{\bullet-}$), photo-generated holes (h^+) and hydroxyl radicals (•OH) to certify the photocatalytic mechanism (Fig. S14) [25, 35]. After adding the same concentration of scavengers, the samples showed different absorbance around 650 nm under the same irradiation time, indicating that the different inhibition effects of the production of oxTMB. And the photocatalytic oxidization of TMB was obviously inhibited especially after adding t-butanol.

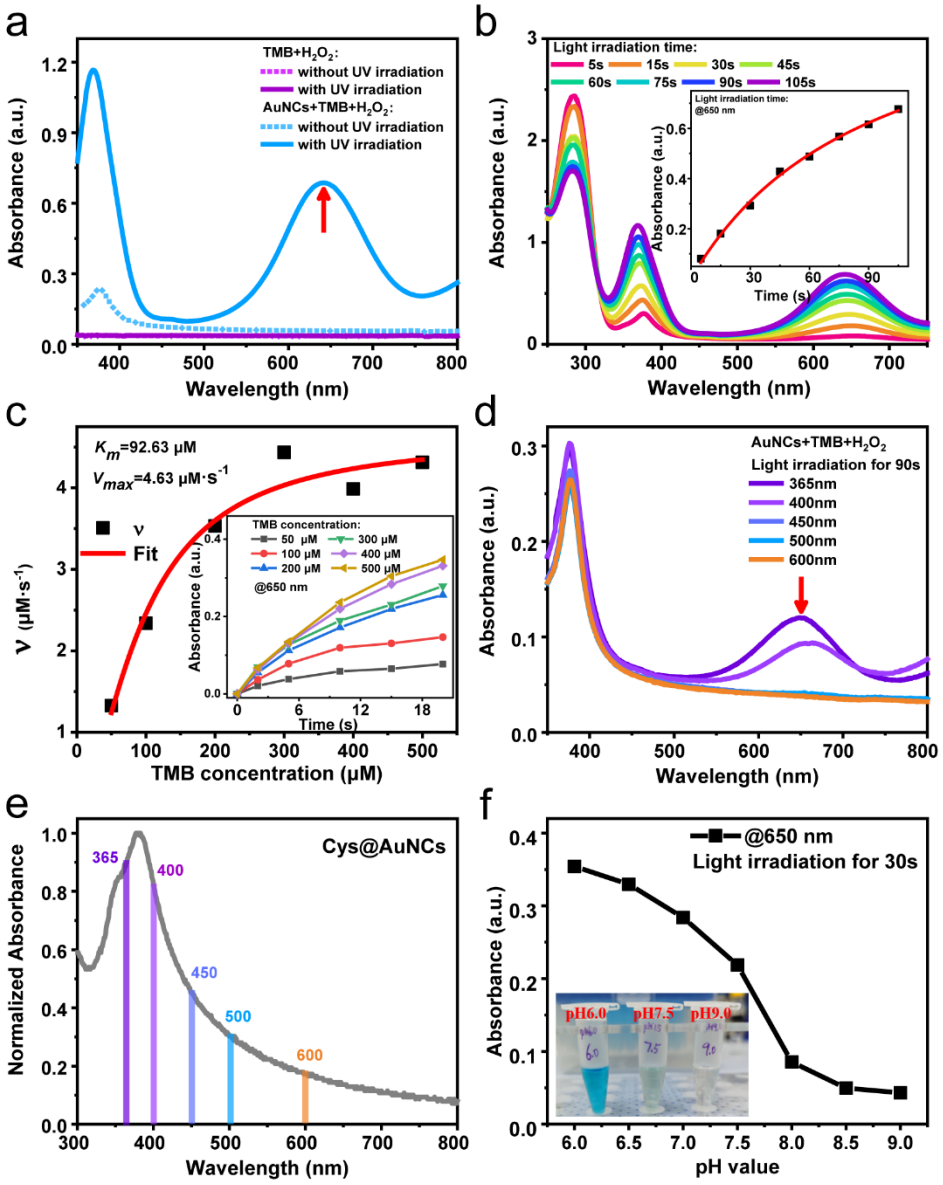

Fig. 4. (a) Effect of nanoclusters and light irradiation on catalytic effect; (b) Photocatalytic reaction rate of nanoclusters. Inset: absorbance at 650 nm as a function of irradiation time; (c) Steady-state kinetic assay of Cys@AuNCs as catalysts under UV irradiation using TMB as the substrate; (d) Catalytic effects of light irradiation at different wavelengths; (e) Positions of irradiation wavelengths in absorption spectrum of Cys@AuNCs; (f) Comparison of the peroxidase-like activity of Cys@AuNCs in different pH values, reaction conditions: 300 μM TMB, 10 μL Cys@AuNCs, 5 mM H_2O_2, irradiation time: 30 s.

4. Conclusions

In this work, we have synthesized cysteine-protected gold nanoclusters (Cys@AuNCs)

by a one-pot water bath, in which cysteine was used as both the reducing and capping agents. The Cys@AuNCs has pH-responsive photoluminescence at ~650 nm, due to the pH-induced aggregation enhanced fluorescence effect. Further by combining with the FITC, a two-photon excited ratiometric luminescent sensor (FITC&Cys@AuNCs) was developed for pH sensing. The pH response interval of the sensor was well matched to the physiological range, and the fluorescence ratio provided a 200-fold variation range for pH measurements. Because of the excellent selectivity, biocompatibility and photostability, FITC&Cys@AuNCs was proved to be a powerful tool for fluorescent imaging and quantitative measurement of pH in living cells under two-photon excitation. Furthermore, Cys@AuNCs also exhibited as efficient photoactivated peroxidase with higher catalytic activity than reported nanomaterial-based peroxidase mimics. More importantly, the photoactivated peroxidase-like activity of Cys@AuNCs allows the control of catalytic reactions through light stimulation. Based on these properties, we believe that the as-synthesized Cys@AuNCs could be widely used in analytical chemistry and photocatalytic.

Appendix A. Supplementary data

Experimental methods and data analysis, Supplementary Figures S1−S14 and Supplementary Tables S1-S3 (PDF)

Author Information

Corresponding Author

* Correspondence to

S.Z. (email: sjzhang@phy.ecnu.edu.cn), R.A (email: rodolphe.antoine@univ-lyon1.fr), and K. Z. (email: kzhang@chem.ecnu.edu.cn)

Acknowledgements

This work was supported by the National Natural Science Foundation of China (12174114 and 21827814), Shanghai Science and Technology Innovation Program (22520712500), “the Research Funds of Happiness Flower ECNU (2021ST2110)”, and “the Fundamental Research Funds for the Central Universities”.

Declaration of interests

The authors declare that they have no known competing financial interests or personal relationships that could have appeared to influence the work reported in this paper.

CRediT author statement

Yuchi Cheng: Conceptualization, Methodology, Data curation, Visualization, Software, Formal analysis, Writing – original draft, Writing – review & editing. **Huangmei Zhou:** Writing – review & editing. **Jinming Xu:** Writing – review & editing. **Yu Zhao:** Data curation. **Xihang Chen:** Writing – review & editing. **Rodolphe Antoine:** Conceptualization. **Meng Ding:** Data curation. **Kun Zhang:** Conceptualization. **Sanjun Zhang:** Conceptualization, Methodology, Validation, Data curation, Funding acquisition, Supervision, Writing - Review & Editing.

References

[1] I. Chakraborty, T. Pradeep, Atomically Precise Clusters of Noble Metals: Emerging Link between Atoms and Nanoparticles, Chemical Reviews, 117 (2017) 8208-8271.

[2] J. Zheng, P.R. Nicovich, R.M. Dickson, Highly fluorescent noble-metal quantum dots, Annual Review of Physical Chemistry, 58 (2007) 409-431.

[3] J.Z. Yan, H.F. Su, H.Y. Yang, C.Y. Hu, S. Malola, S.C. Lin, B.K. Teo, H. Hakkinen, N.F. Zheng, Asymmetric Synthesis of Chiral Bimetallic $[Ag28Cu12(SR)24]^{4-}$ Nanoclusters via Ion Pairing, Journal of the American Chemical Society, 138 (2016) 12751-12754.

[4] M.Z. Zhu, C.M. Aikens, M.P. Hendrich, R. Gupta, H.F. Qian, G.C. Schatz, R.C. Jin, Reversible Switching of Magnetism in Thiolate-Protected Au_{25} Superatoms, Journal of the American Chemical Society, 131 (2009) 2490-2492.

[5] S.W. Chen, R.S. Ingram, M.J. Hostetler, J.J. Pietron, R.W. Murray, T.G. Schaaff, J.T. Khoury, M.M. Alvarez, R.L. Whetten, Gold nanoelectrodes of varied size: Transition to molecule-like charging, Science, 280 (1998) 2098-2101.

[6] S.Y. Qian, Z.P. Wang, Z.X. Zuo, X.M. Wang, Q. Wang, X. Yuan, Engineering luminescent metal nanoclusters for sensing applications, Coordination Chemistry Reviews, 451 (2022) 25.

[7] G. Li, R. Jin, Atomically Precise Gold Nanoclusters as New Model Catalysts, Accounts of Chemical Research, 46 (2013) 1749-1758.

[8] Z. Qiao, J. Zhang, X. Hai, Y. Yan, W. Song, S. Bi, Recent advances in templated synthesis of metal nanoclusters and their applications in biosensing, bioimaging and theranostics, Biosensors and Bioelectronics, 176 (2021) 112898.

[9] J.T. Hou, W.X. Ren, K. Li, J. Seo, A. Sharma, X.Q. Yu, J.S. Kim, Fluorescent bioimaging of pH: from design to applications, Chemical Society Reviews, 46 (2017) 2076-2090.

[10] B.A. Webb, M. Chimenti, M.P. Jacobson, D.L. Barber, Dysregulated pH: a perfect storm for cancer progression, Nature Reviews Cancer, 11 (2011) 671-677.

[11] T.A. Davies, R.E. Fine, R.J. Johnson, C.A. Levesque, W.H. Rathbun, K.F. Seetoo, S.J. Smith, G. Strohmeier, L. Volicer, L. Delva, E.R. Simons, Non-age-related differences in thrombin responses by platelets from male-patients with advanced alzheimers-disease, Biochemical and Biophysical Research Communications, 194 (1993) 537-543.

[12] F.B. Loiselle, J.R. Casey, Measurement of Intracellular pH, Membrane Transporters in Drug Discovery and Development: Methods and Protocols, Humana Press Inc, 999 Riverview Dr, Ste 208, Totowa, Nj 07512-1165 USA, 2010, pp. 311-331.

[13] R. Ali, S.M. Saleh, S.M. Aly, Fluorescent gold nanoclusters as pH sensors for the pH 5 to 9 range and for imaging of blood cell pH values, Microchimica Acta, 184 (2017) 3309-3315.

[14] C.Q. Ding, Y. Tian, Gold nanocluster-based fluorescence biosensor for targeted imaging in cancer cells and ratiometric determination of intracellular pH, Biosensors & Bioelectronics, 65 (2015) 183-190.

[15] J. Olesiak-Banska, M. Waszkielewicz, P. Obstarczyk, M. Samoc, Two-photon absorption and photoluminescence of colloidal gold nanoparticles and nanoclusters, Chemical Society Reviews, 48 (2019) 4087-4117.

[16] I. Russier-Antoine, F. Bertorelle, M. Vojkovic, D. Rayane, E. Salmon, C. Jonin, P. Dugourd, R. Antoine, P.F. Brevet, Non-linear optical properties of gold quantum clusters. The smaller the better, Nanoscale, 6 (2014) 13572-13578.

[17] V. Bonacic-Koutecky, R. Antoine, Enhanced two-photon absorption of ligated silver and gold nanoclusters: theoretical and experimental assessments, Nanoscale, 11 (2019) 12436-12448.

[18] C. Xu, W. Zipfel, J.B. Shear, R.M. Williams, W.W. Webb, Multiphoton fluorescence

excitation: New spectral windows for biological nonlinear microscopy, Proceedings of the National Academy of Sciences of the United States of America, 93 (1996) 10763-10768.

[19] N.C. Veitch, Horseradish peroxidase: a modern view of a classic enzyme, Phytochemistry, 65 (2004) 249-259.

[20] F. Manea, F.B. Houillon, L. Pasquato, P. Scrimin, Nanozymes: Gold-nanoparticle-based transphosphorylation catalysts, Angewandte Chemie-International Edition, 43 (2004) 6165-6169.

[21] X. Jiang, C.J. Sun, Y. Guo, G.J. Nie, L. Xu, Peroxidase-like activity of apoferritin paired gold clusters for glucose detection, Biosensors & Bioelectronics, 64 (2015) 165-170.

[22] Q. Zhao, H. Yan, L. Ping, Y.Y. Yao, Y.D. Wu, J. Zhang, H.X. Li, X.Q. Gong, J. Chang, An ultra-sensitive and colorimetric sensor for copper and iron based on glutathione-functionalized gold nanoclusters, Analytica Chimica Acta, 948 (2016) 73-79.

[23] Borghei, Y.S., Hosseini, M. & Ganjali, M.R. Oxidase-like Catalytic activity of Cys-AuNCs upon visible light irradiation and its application for visual miRNA detection. Sensors and Actuators B-Chemical. 273 (2018), 1618-1626.

[24] Wang, G.L., Jin, L.Y., Dong, Y.M., Wu, X.M. & Li, Z.J. Intrinsic enzyme mimicking activity of gold nanoclusters upon visible light triggering and its application for colorimetric trypsin detection. Biosensors & Bioelectronics. 64 (2015) 523-529.

[25] X.X. Su, J.B. Liu, pH-Guided Self-Assembly of Copper Nanoclusters with Aggregation-Induced Emission, Acs Applied Materials & Interfaces, 9 (2017) 3902-3910.

[26] Wang, X. Y. Feng, J. Liu, K. Cheng, Y. Liu, W. Yang, H. Zhang, H. Peng. Fluorescein isothiocyanate-doped conjugated polymer nanoparticles for two-photon ratiometric fluorescent imaging of intracellular pH fluctuations. Spectrochimica acta. Part A, Molecular and biomolecular spectroscopy, 267 (2022) 120477.

[27] D. Xu, Y.H. Li, C.Y. Poon, H.N. Chan, H.W. Li, M.S. Wong, A Zero Cross-Talk Ratiometric Two-Photon Probe for Imaging of Acid pH in Living Cells and Tissues and Early Detection of Tumor in Mouse Model, Analytical Chemistry, 90 (2018) 8800-8806.

[28] B. Kong, A.W. Zhu, C.Q. Ding, X.M. Zhao, B. Li, Y. Tian, Carbon Dot-Based Inorganic-Organic Nanosystem for Two-Photon Imaging and Biosensing of pH Variation in Living Cells and Tissues, Advanced Materials, 24 (2012) 5844-5848.

[29] A. Ray, Y.E.K. Lee, T. Epstein, G. Kim, R. Kopelman, Two-photon nano-PEBBLE sensors: subcellular pH measurements, Analyst, 136 (2011) 3616-3622.

[30] S. Kim, H.E. Pudavar, P.N. Prasad, Dye-concentrated organically modified silica nanoparticles as a ratiometric fluorescent pH probe by one- and two-photon excitation, Chemical Communications, 19 (2006), 2071-2073.

[31] M. Matulionyte, D. Dapkute, L. Budenaite, G. Jarockyte, R. Rotomskis, Photoluminescent Gold Nanoclusters in Cancer Cells: Cellular Uptake, Toxicity, and Generation of Reactive Oxygen Species, International Journal of Molecular Sciences, 18 (2017) 17.

[32] J. Guo, A.S. Rubfiaro, Y.H. Lai, J. Moscoso, F. Chen, Y. Liu, X.W. Wang, J. He, Dynamic single-cell intracellular pH sensing using a SERS-active nanopipette, Analyst, 145 (2020) 4852-4859.

[33] L. Su, J. Feng, X.M. Zhou, C.L. Ren, H.H. Li, X.G. Chen, Colorimetric Detection of Urine Glucose Based $ZnFe_2O_4$ Magnetic Nanoparticles, Analytical Chemistry, 84 (2012) 5753-5758.

[34] X.L. Fan, B. Cai, R. Du, R. Hubner, M. Georgi, G.C. Jiang, L.W. Li, M.S. Khoshkhoo, H.J. Sun, A. Eychmuller, Ligand-Exchange-Mediated Fabrication of Gold Aerogels Containing. Different Au(I) Content with Peroxidase-like Behavior, Chemistry of Materials, 31 (2019) 10094-10099.

[35] G.X. Cao, X.M. Wu, Y.M. Dong, Z.J. Li, G.L. Wang, Colorimetric determination of melamine based on the reversal of the mercury (II) induced inhibition of the light-triggered oxidase-like activity of gold nanoclusters, Microchimica Acta, 183 (2016) 441-448.